Adsorption of Thymine on Gold Single-Crystal Electrodes

B. Roelfs,[†] E. Bunge,[†,‡] C. Schröter,[†] T. Solomun,[†] H. Meyer,[‡] R. J. Nichols,[§] and H. Baumgärtel*,[†]

Freie Universität Berlin, Takustrasse 3, 14195 Berlin, Germany, Atotech Deutschland GmbH, Erasmusstrasse 20-24, 10553 Berlin, Germany, and Department of Chemistry, The University of Liverpool, Liverpool L69 3BX, U.K.

Received: June 19, 1996; In Final Form: September 24, 1996[⊗]

We have examined the adsorption of thymine on (111), (100), and (210) gold single-crystal surfaces. The adsorption behavior on these three surfaces has been investigated by classical electrochemical methods like cyclic voltammetry and capacitance−potential measurements. Additionally *in situ* scanning tunneling microscopy (STM) and *ex situ* photoelectron spectroscopy (XPS) measurements have been performed for the adsorption of thymine on the (111) surface. The capacitance measurements as well as cyclic voltammetry investigations show the three adsorption states of thymine on all Au electrodes. The first adsorption state refers to a random adsorption of thymine molecules at negative surface charges. The second state can be characterized as a condensed but weakly adsorbed adlayer on the (100) and (111) crystals, whereas a noncondensed state has been found on the (210) surface. The condensed thymine film is stabilized mainly by hydrogen bonding. High-resolution STM images for this film on the (111) electrode point to an ordered adlayer with a unit cell which is incommensurate with the underlying Au surface. The images indicate flat adsorbing thymine molecules in this state. The third adsorption state is characterized by charge transfer from deprotonated thymine molecules to the gold surface. XPS data show one chemically modifed nitrogen atom for the chemisorbed thymine film. This adsorption state shows a commensurate $2\sqrt{3} \times 2\sqrt{3}$ overstructure in the STM image. The STM images are interpreted by stacks of adsorbed thymine molecules with the molecular plane perpendicular to the surface. The stacks are connected by coadsorbed water molecules. The molecules are bound by a deprotonated nitrogen to the surface.

1. Introduction

Many molecules organize spontaneously into ordered monolayers at very different interfaces, including the liquid/solid and liquid/liquid interface. Adsorption to form well-ordered or self-assembled adlayers occurs from solutions under both electrochemical and nonelectrochemical conditions. There are many examples in the literature, for instance, the adsorption of nanoic acid,[1] pyridine,[2] and campher[3,4] on a liquid mercury electrode. The formation of ordered organic adlayers on solid surfaces has been observed for thiols,[5] pyrimidines,[6,7] and purines,[6,7] mostly under nonelectrochemical conditions. *In situ* electrochemical investigations on solid electrodes have also been reported for the purines and pyrimidines,[8−11] pyridine,[12] and uridine.[13] These electrochemical systems have been extensively investigated over the last few decades, mainly by classical methods such as cyclic voltammetry, capacitance measurements, and current transients. Such measurements can yield information about the initiation of such films and in some cases, when used in conjunction with themodynamic analysis, of the packing densities of the adsorbed molecules. Armstrong[2] could describe the evolution of an ordered pyridine layer on a dropping mercury electrode (dme) with a simultaneous nucleation and growth mechanism. The mechanisms of nucleation and growth of organic films on electrodes continue to stimulate much research interest (see, e.g., refs 14 and 15 and references therein). In some cases, it is possible to apply nucleation and growth mechanisms that were originally developed for the electrodeposition of metals. Packing densities could also be estimated in certain cases, and here, it could be determined whether the adsorbed molecule adopts an orientation perpendicular, parallel, or tilted to the surface.[16]

With the development of new surface-sensitive tools, new insights into geometry, film compositions, and binding states have become available. In this respect, techniques of particular relevance include surface-enhanced Raman scattering,[17,18] interfacial infrared measurements,[19−21] scanning tunneling microscopy,[22,23] and *ex situ* ultrahigh vacuum studies.[24,25]

These techniques reveal different mechanisms and driving forces for the formation of ordered monolayers. Well-characterized examples include long-chain thiols which often adopt a $\sqrt{3} \times \sqrt{3}$ *R*30° geometry on a Au(111) surface. This mainly reflects the very strong interaction between the sulfur atom and the gold surface in that it allows the sulfur to occupy a 3-fold hollow site. Very similar behavior is shown by other sulfur-containing molecules. We recently showed a (3×3) adsorption geometry for tetramethylthiourea (TMTU) on Au(111).[26,27] In this particular case, the interaction between gold and sulfur is so strong that it leads to a slow etching of the surface at positive potentials.

Compounds such as purines and pyrimidines interact generally more weakly with the substrate surface than molecules which contain sulfur. For these molecules, it is assumed that the ordered monolayer is stabilized by interaction between the molecules, for instance, by the development of hydrogen-bonding networks. In the case of pyrimidines, it has been found that their interaction or adsorption behavior on solid electrodes can change with the applied potential. In particular, uracil and thymine (see Figure 1) molecules are known to adsorb in a weakly as well as in a strongly bound adsorption state.[10,28] The adsorption geometries of these films are unknown. The change in the adsorption state has been explained by charge transfer

[†] Freie Universität Berlin.
[‡] Atotech Deutschland GmbH.
[§] The University of Liverpool.
[⊗] Abstract published in *Advance ACS Abstracts,* January 1, 1997.

S1089-5647(96)01814-7 CCC: $14.00 © 1997 American Chemical Society

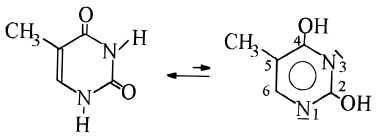

Figure 1. Tautomeric forms of thymine.

from adsorbed thymine molecules to the substrate,[9,28] but clear evidence fails. This paper deals mainly with the two different adsorption states of thymine on different Au surfaces. We address here primarily the structural nature of the adsorbed films. In particular, the role of coadsorbed water is examined and the driving force behind the change in adsorption states is analyzed.

This paper is organized into three main parts. The first part deals with the electrochemical characterization of thymine adsorption on the different Au single-crystal electrodes. In the second part, we present *ex situ* photoelectron measurements of a Au(111) surface after emersion from thymine-containing solutions. We will discuss the binding states of adsorbed thymine. In the third part, we present *in situ* STM measurements of the thymine-covered Au(111) surface and deduce an adsorption model.

2. Experimental Section

2.1. Instrumentation. The capacitance has been measured using the lock-in technique. The applied potential was controlled by an EG&G PAR 273 potentiostat. To this potential, an ac voltage with a constant amplitude of 5 mV and frequency of 80 Hz, generated by the internal wave form generator of a lock-in amplifier (EG&G 5210), was superimposed. The imaginary and real parts of the current response were transformed into dc voltage and recorded simultaneously by a two-channel storage oscilloscope with a 1-mV potential resolution.

XPS measurements were performed after sputtering and annealing of the crystal. The crystal was then transferred to a second vacuum chamber, which is linked via a valve to the electrochemical compartment. After the electrochemical measurements, under argon atmosphere, the crystal was immediately retransferred to the UHV chamber. XP spectra were recorded after a waiting period of about 15−20 min, when a pressure of about 10^{-8} mbar had been reached. Data were obtained by Al Kα radiation using a hemispherical analyzer (VG) with a pass energy set to 20 eV. Energy calibration was accomplished by referencing to the Au($4f_{7/2}$) level at 83.8 eV.

The STM imaging has been performed with a Topometrix TMX 2000 STM with a bipotentiostat. We used $Pt_{0.8}Ir_{0.2}$ tips, coated with nail polish (Ellen Betrix).

2.2. Electrodes. The Au single-crystal electrodes, which we used for the electrochemical measurements, were grown, cut, and polished at LEI, CNRS in Meudon, France. The (111) single crystal for the *ex situ* measurements was prepared in the Fritz-Haber-Institut in Berlin. The working electrode for the STM measurements consists of a 200-nm-thick gold film vacuum evaporated onto Tempax glass with a 2-nm-thick chromium underlayer (Berliner Glass KG). This latter kind of electrode shows large terraces of (111) orientation.[29,30] The electrodes for the STM and electrochemical measurements were heated in a Bunsen burner to red heat and cooled in pure argon or quenched with triply distilled water. In all cases, platinum wires serve as counter electrodes. Ag wire reference electrodes were used in the STM cell and for the *ex situ* XPS measurements. These wires held a stable potential, within a few millivolts, over the course of the measurements. Nevertheless, all potentials mentioned in this article are quoted against the saturated calomel electrode (SCE).

2.3. Substances. Both thymine (Merck >98%) and $KClO_4$ (Merck, ACS grade) have been recrystallized from triply distilled water. The pH variation has been achieved by addition of concentrated $HClO_4$ (70% Merck suprapur) or 1 M potassium hydroxide (Merck titrisol). Other electrolytes (NaF, Merck suprapur, and Na_2SO_4, Merck suprapur) have been used without further purification. Acetonitrile (Baker analyzed) has been distilled over CaH_2 resulting in a water content of about 0.003 vol%, monitored by Carl Fischer titration.

3. Results and Discussion

3.1. Electrochemical Investigations. 3.1.1. Capacitance Measurements and Cyclic Voltammetry: Temperature Dependence. This section begins with the electrochemical investigations of thymine adsorption on all three gold surfaces. Capacitance vs potential plots for a 5 mM thymine solution in 0.1 M $KClO_4$ (pH 5.96) at different temperatures are shown in Figure 2. The dotted curves refer in each case to the capacitance measurements in pure $KClO_4$ containing solutions at 293 K without the addition of thymine. The measurements were performed after immersion of the electrode under potential control and an initial waiting time of 3 min at the negative potential limit.

From Figure 2, one can distinguish three different capacitance regions for all three crystals. The first region at negative potentials ($E < -0.20$ V) shows an increase of the capacitance compared to the pure electrolyte. This can be interpreted by the beginning of the ad- or desorption of randomly adsorbed thymine molecules. Similar ad- and desorption peaks have frequently been observed (see, e.g., ref 31) on various electrode materials. The second adsorption state spans the potential range from around −0.20 up to +0.25 V. This region is marked by a substantial and steep decrease of the capacitance down to 12 μF/cm^2 for both the (100) and the (111) surfaces, whereas the capacitance declines smoothly for the (210) crystal. This capacitance edge occurs only if the concentration of thymine exceeds 1 mM at room temperature. Otherwise, a smooth decline of the capacitance is observed, for which the minimum value of the capacitance depends on the solution concentration of thymine. For the (100) and (111) surfaces, this capacitance region is limited by the steep capacitance edge at negative potentials and by a small peak at 0.25 V at the positive end. This region shows the typical behavior of a condensed adsorption layer for the (100) and (111) surfaces for thymine concentrations $c > 1$ mM, as has been reported for thymine on the dropping mercury electrode.[32−34] It is significant that there is a strong dependence on temperature. Increasing the temperature results in a positive shift of the negative capacitance edge. The sharp capacitance edge vanishes at 328 K on both surfaces, indicating the dissolution of the condensed adlayer. We have found a very similar capacitance behavior by variation of the thymine concentration (not shown here). As mentioned above, thymine concentrations of $c > 1$ mM at $T = 293$ K are necessary to observe a similar capacitance edge. This strong temperature and concentration dependence point to a weakly adsorbed thymine film. In the following discussion, we use the expression "physisorbed film" to distinguish this kind of film from the film which is observed in the third potential region.

The third adsorption region, at potentials $E > 0.25$ V, shows a negligible temperature dependence of the capacitance for all surfaces. The capacitance reaches a low and constant value of 10 μF/cm^2, which is slightly but significantly lower than in the second region (physisorbed film). Up to now, there is no quantitative relationship known between the absolute value of the capacitance and the structure of the adsorbate. This is due

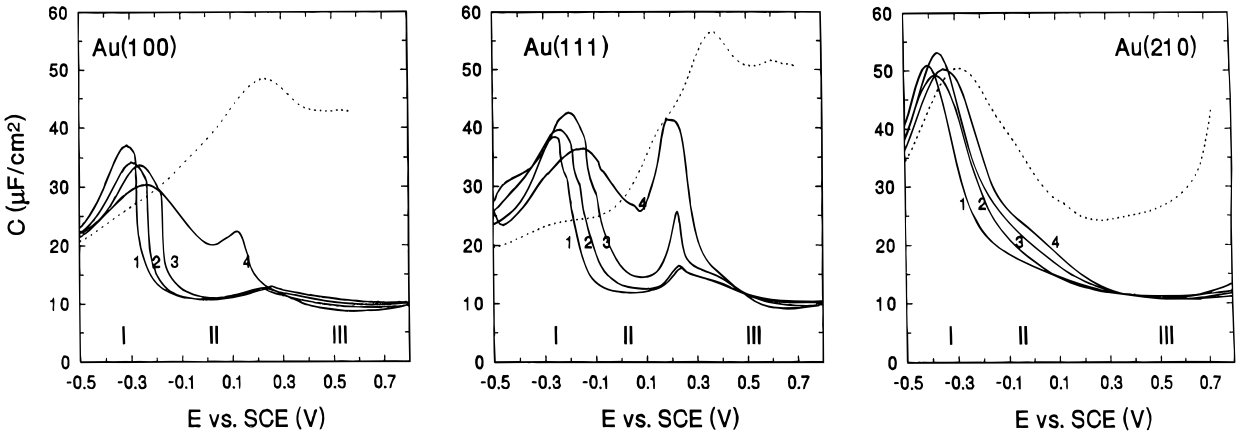

Figure 2. Capacitance vs potentials plots for Au(*hkl*) surfaces in 5 mM thymine and 100 mM $KClO_4$ for different temperatures. The dotted line represents the electrolyte without thymine at 293 K. Sweep rate, 2 mV/s; positive sweep direction, (1) $T = 283$ K, (2) $T = 293$ K, (3) $T = 303$ K, and (4) $T = 333$ K.

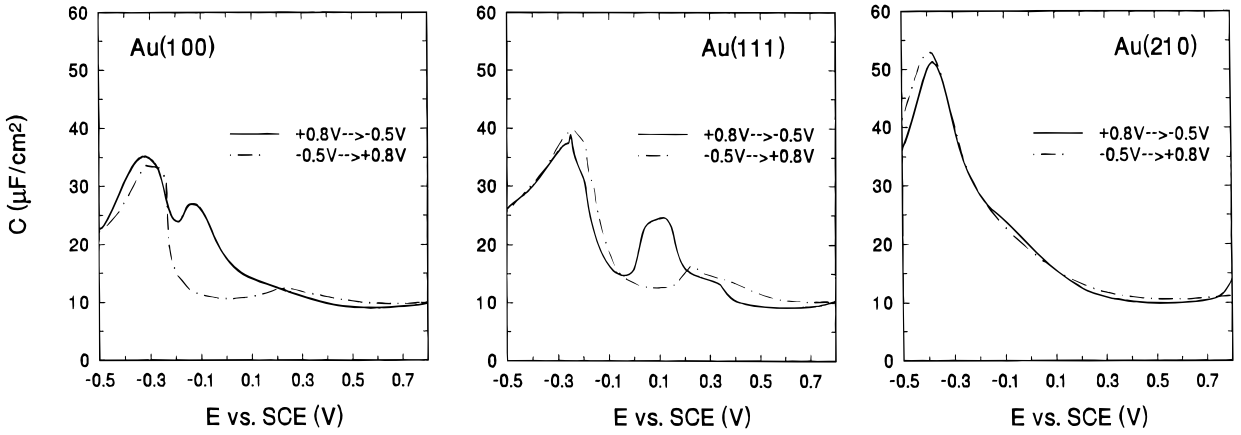

Figure 3. Capacitance vs potentials plots for a Au(*hkl*) surfaces in 5 mM thymine and 100 mM $KClO_4$ for different sweep directions at 293 K. The full line represents the negative sweep direction: sweep rate, 2 mV/s.

to changes of the dielectric constant in the double layer and to changes in the polarizability of the adsorbate molecules with potential. Therefore, it is not possible to extract structural or binding parameters solely on the basis of the saturation value of our capacitance data. This will be done on the basis of STM measurements in the following chapters. Nevertheless, some conclusions from the temperature and thymine concentration dependence of the capacitance can be drawn. Our data show no evidence for the dissolution of this adsorption layer (region III) in the available temperature region (up to 338 K). The saturation capacitance of 10 μF/cm^2 can also be observed in very low concentration thymine solutions (even at $c = 10^{-6}$ M thymine, not shown here). This behavior suggests a very strong adsorption of thymine molecules. For further discussion, we will call this the "chemisorbed film". The reason for the stability of this thymine film will be discussed latter in this paper.

The overall capacitance vs potential plots do not show any difference if we substitute $KClO_4$ by Na_2SO_4 or NaF. Therefore, we can exclude any coadsorption of anions or cations in the physisorbed and chemisorbed film.

The capacitance vs potential plots show a substantial "hysteresis" between the positive and negative potential scans (Figure 3) for the (100) as well as for the (111) surface. All capacitance measurements have been performed after an immersion of the electrodes under potential control and an additional waiting period of 3 min at the negative potential scale. The hysteresis occurs on both surfaces if a "critical" potential of +0.2 V is exceeded. Only a negligible hysteresis in the ad/desorption region at the negative potential region has been found for the (210) surface. This kind of hysteresis for both former surfaces has been explained by Kolb and co-workers[35] in terms of reconstruction phenomena. A reconstructed surface shows a rearrangement of its topmost atomic layers to form a surface lattice different from the underlying bulk crystallography. It is now well established that the (100) and the (111) Au surfaces are reconstructed in electrolyte solutions under certain conditions: the crystals have to be immersed at negative potentials after flame annealing, and strong adsorption of ions or organic molecules should be avoided, since they tend to lift the reconstruction.[35] The reconstruction leads to the so-called (100) (5×20) and (111) ($\sqrt{3}\times22$) surfaces which show very similar characteristics concerning the potential of zero charge (Epzc) and work function.[35] The transformation from the unreconstructed to the reconstructed surface has not only been induced by flame annealing but also by polarizing the electrode surface negatively. The time scale for this transformation is different for the (111) and the (100) surfaces. In the former case, reversible behavior is observed, whereas the transformation in the latter case occurs on a significantly larger potential and time scale (minutes to hours). Up to now, there is no evidence for a reconstruction of the (210) surface, either in ultrahigh vacuum or in electrolyte solutions.

These facts provide a framework for the interpretation of the capacitance measurements. For the (210) crystal, we observe a unique (1×1) surface structure over the entire potential range, as can be suggested by the absence of a significant hysteresis. Thymine molecules adsorb randomly at negative potentials and chemisorb at positive potentials. For the (100) and (111)

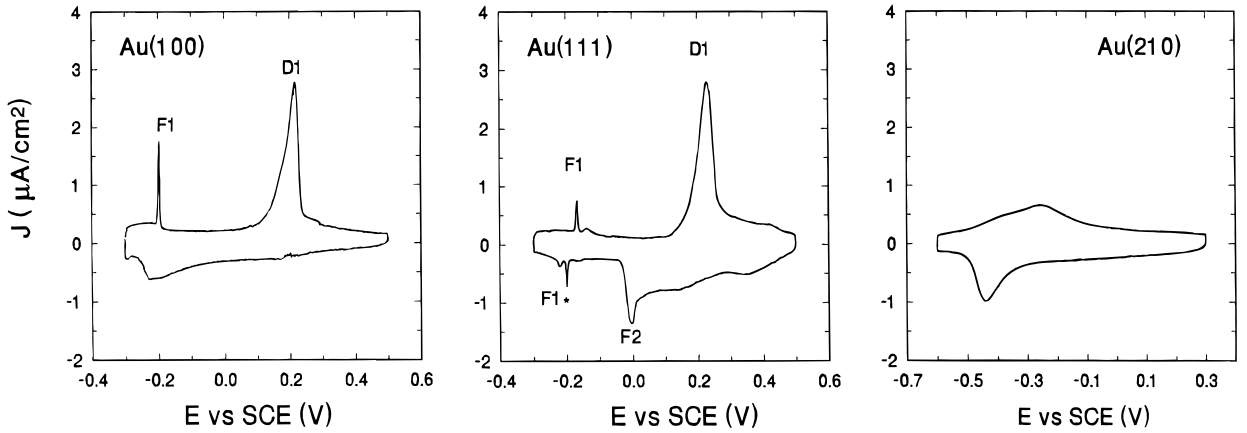

Figure 4. Cyclic voltammograms for Au(*hkl*) surfaces in 5 mM thymine and 100 mM $KClO_4$. Sweep rate is 5 mV/s after potential-controlled immersion of the electrode at the negative potential limit and an initial waiting period of 3 min at the same potential.

surface, a transformation from the reconstructed into the unreconstructed surface at the critical potential $E = +0.2$ V, occurs. Therefore, we have to assume that the physisorbed film in region II is formed at the negatively polarized and reconstructed surface. In fact, we did not observe sharp capacitance edges for the (100) surface, which indicates film formation if a negative potential scan was applied. The same observation has been made by immersing the electrode without potential control and starting the measurement at the negative potential end by using a past positive scan ($dE/dt > 10$ mV/s). In this case, the time scale in which the electrode surface is polarized negatively is too short to induce the reconstruction of the surface. An analogous adsorption behavior of uracil has been reported by Hölzle et al.[36] These authors have shown that a physisorbed film of uracil might also be stable on unreconstructed but smooth and island-free Au(100) surfaces. Lifting of the reconstruction leads normally (also in our case) to a gold-island-covered surface which destabilizes the film formation by reducing lateral attractive interactions of adsorbed molecules. The chemisorbed film at positive electrode potentials is probably formed on the unreconstructed (100) surface. This is likely to be the case for the (111) surface. Since the physisorbed film on the (111) surface in region II is observed at potentials negative from the critical potential, we suppose that it is formed also on the reconstructed surface.

The formation of condensed adlayers can also be monitored by cyclic voltammetry. The formation of a condensed film can be interpreted as a phase transition in the adlayer from randomly adorbed to highly ordered thymine molecules. This kind of phase transition leads to sharp and symmetrically shaped peaks in the voltammograms.[37]

Voltammograms for the three surfaces after immersion under potential control and an initial waiting period of 3 min at the negative potential limits are shown in Figure 4. The most striking features in the voltammograms are the existence of very sharp peaks for the (100) and (111) surface, whereas no such peaks are visible for the (210) crystal. We denote these peaks as F1 and D1 since they are related to different processes. All peaks show a linear increase of their maximum with the scan rate, indicating capacitive currents or Faradaic currents which are restricted to adsorbed species. The peaks F1, F1*, and F2 in the voltammograms for the (100) and (111) surfaces are related to the formation of a condensed physisorbed film of thymine. Again, these peaks occur only if the solution concentration of thymine exceeds 1 mM at room temperature. For lower thymine concentrations for which the capacitance curves lend support to the conclusion that thymine is randomly adsorbed, no such peaks are observed. Moreover, the peak

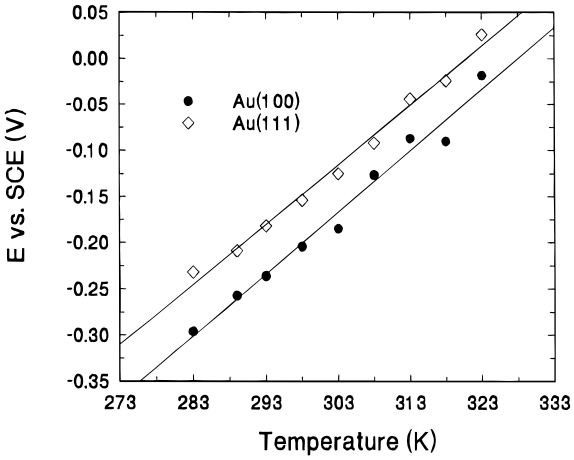

Figure 5. Shift of peak F1 with temperature obtained by cyclic voltammetry. Full circles represent the Au(100) surface, open diamonds the Au(111) surface.

positions of F1 are coincident with the potentials of the capacitance edges in Figure 2. The appearances of F1* and F2 are closely linked with the occurrence of F1. The form of these peaks indicates that the film formation or dissolution depends on the applied potential program. Peak F1 occurs nearly at the same potential at -0.205 ± 0.010 V for the (100) surface and at -0.180 ± 0.010 V for the (111) surface. The extremely small charge of about $2-3\ \mu C/cm^{-2}$ connected with these peaks lends support to a film formation of uncharged species. The full width at half-maximum (FWHM) of F1 is only 4.5 ± 0.5 mV (100) and 6.5 ± 0.5 mV (111). Peak F1*, which is related to the film dissolution, occurs also for the (100) surface if the potential is kept negative of peak D1 (not shown here). Peak F1 is very sharp and, hence, provides a more accurate indicator of the transition potential from randomly adsorbed thymine to the physisorbed layer than can be obtained from the capacitance measurements. The dependence of this peak potential of F1 on temperature is shown in Figure 5. A linear shift of 6.6 ± 0.3 mV/K of F1 is obtained for both surfaces. The peaks vanish at a critical temperature of 328 K on both surfaces.

The absence of any sharp peaks F_i in the voltammogram for the (210) surface is more clear evidence for the absence of a physisorbed condensed adlayer on this surface. Scharfe et al.[13] reported a very similar crystallographic effect on the film formation of uridine. Up to now, it was not clear whether this is a geometric or electronic effect on the (210) surface. Further measurements on different crystallographic planes of gold would be helpful.

The other D1 peaks in the voltammograms of the (111) and (100) surfaces are much more difficult to relate to single processes. The charge under these peaks is 29 ± 4 μC/cm^{-2} (100) and 41 ± 4 μC/cm^{-2} (111) and as such is too high to be related to pure capacitive currents which might arise from a reorganization in the double layer. In pure $KClO_4$-containing solutions, we observed similar peaks at 0.50 V (Au(100)) and 0.32 V (Au(111)) with significantly lower charges of about 4 ± 1 μC/cm^{-2} for both surfaces. These latter peaks in pure electrolyte are interpreted as arising the lifting of the reconstruction.[35]

In fact, the peak position of D1 is equivalent to the critical potential where the capacitance hysteresis occurs. Therefore, we assume that the reconstruction is indeed lifted in the process which is characterized by D1. The reconstruction itself causes an additional recharging of the surface since the Epzc is changed within a few milliseconds. The difference between the Epzc for the reconstructed and unreconstructed surfaces is for the (100) surface with 220 mV about 2.5 times higher than for the (111) surface with 90 mV. Hence, if lifting of the reconstruction is the only contribution to the recharging of the double layer, one would expect a significantly higher current for the (100) surface than for the (111) surface. In fact, the opposite is observed. Moreover, one can estimate with a very simple method the charge flow that is associated with the change in the Epzc during the lifting of the reconstruction. The charge q is related to the capacitance by eq 1. If the capacitance does

$$q = \int_{E1}^{E2} C \, dE \tag{1}$$

not change dramatically during the transformation, then it is reasonable to estimate the charge associated with the reconstruction by using a mean capacitance, derived from the average of the capacitance before and after lifting the reconstruction. Using C_m = 15 μF/cm^{-2} gives a charge value of only 3.3 μC/cm^{-2} for the (100) surface and 1.35 μC/cm^{-2} for the (111) surface. This seems definitely too low to account for the charge under peak D1. A possible desorption of the organic molecules during the surface transformation should result in intermediate capacitance values of about 50 μF/cm^{-2} (see dotted lines in Figure 2), giving rise to charge values of about 11 μC/cm^{-2} for Au(100) and 4.5 μC/cm^{-2} for Au(111). These values are still too low. This analysis implies that neither lifting of the reconstruction nor total desorption of the organic molecule can be the major contribution to the charge associated with peak D1.

We therefore believe that an additional charge-transfer process is responsible for the charge connected with D1. In this respect, Tao et al. have also proposed a charge transfer from adsorbed thymine molecules to the Au(111) surface.[9]

The analogous analysis for the Au(210) surface lacks somewhat from a precise measurement of the relating charge since a sharp and symmetrically shaped peak fails. The charge-transfer process seems to run parallel with the progressive adsorption of thymine at negative potentials. The charge under this peak can only roughly be estimated to about 21 ± 7 μC/cm^{-2}. The temperature dependence of D1 is negligible for all three surfaces, which also points to a charge-transfer process rather than pure capacitive currents.

3.1.2. pH Variations. In order to obtain further information about the charge-transfer process, the pH of the solutions was varied by adding KOH or $HClO_4$. Figure 6 shows the dependence of D1 on solution pH. It is significant that the peak position of D1 is similar for both surfaces. In the pH range from 4 to 10, we observe a linear shift of −72 ± 5 mV/pH unit. At a lower pH, a constant peak position for D1 of 0.37 ± 0.01 V is obtained.

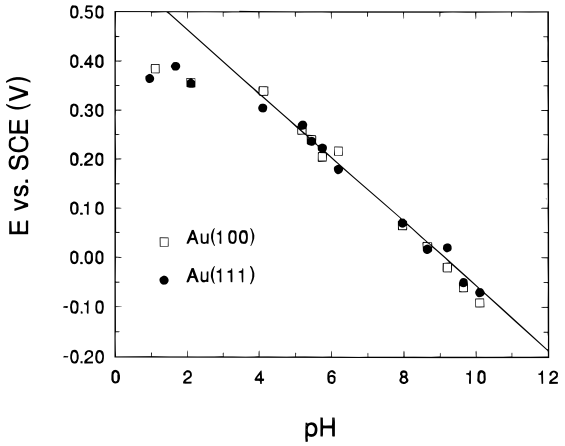

Figure 6. Shift of peak D1 with pH changes of the solutions obtained by cyclic voltammetry. Full circles represent the Au(111) surface, open squares the Au(100) surface.

The following mechanism could account for the observed pH dependence of D1:

$$RNH_{solution} \Leftrightarrow RNH_{adsorbed} \tag{a}$$

$$RNH_{adsorbed} \Leftrightarrow RN^{-(1-n)}{}_{adsorbed} + H^+(aq) + ne^- \tag{b}$$

This reaction scheme would not only explain the pH dependence and the charge due to the formation of anionic species in step b but also the high-temperature stability of the chemisorbed film. Further evidence for such a mechanism comes from Manousek and Zuman,[38] who measured an anodic polarographic activity of thymine and uracil only for their anionic form. These authors assigned the anodic polarographic wave to the transfer of about one electron. The deprotonation in step b is likely to occur at N(3) (see Figure 1). This NH group shows extraordinary low pK's of 9.5[39] or 9.94[40] due to the mesomeric stabilization of the anion. Similar to the evaluation of the one-electron redox behavior of the purines and pyrimidines by Jovanovic and Simic[41] and the adsorption of sulfate ions on gold (111) by Angerstein-Kozlowska et al.,[42] we assume that the potential shift of D1 can be expressed by

$$\Delta E_{D1} = 0.059/n \log[H^+] = -0.059/n\text{pH} \tag{2}$$

where n equals the number of transferred electrons. From Figure 5, we calculate a shift of 72 ± 5 mV, leading to n = 0.81 ± 0.06 electrons. Clearly, n should be 1 if every adsorbed thymine molecule eliminates a proton. However, this deviation from ideality is not too great or unexpected, since peak D1 does not consist merely of one simple ideal surface redox process. The analysis can be extended to estimate a limiting value for the surface excess Γ_m of thymine in the chemisorbed film by applying

$$q_{D1} = nF\Gamma_m \tag{3}$$

From eq 3, we estimate a Γ_m of (5.2 ± 0.6) × 10^{-10} mol cm^{-2} for Au(111), (3.7 ± 0.5) × 10^{-10} mol cm^{-2} for Au(100), and (2.8 ± 0.9) × 10^{-10} mol cm^{-2} for Au(210). These values only represent upper limiting values for the chemisorbed films since the capacitive contributions to the charge in D1 due to reorganization effects are not considered. The value of Γ_m for the Au(111) surface points to a densely packed monolayer in which the molecules adopt an orientation with their molecular planes perpendicular to the surface. In the case of the (100) surface, the surface excess is in full agreement with a thymine

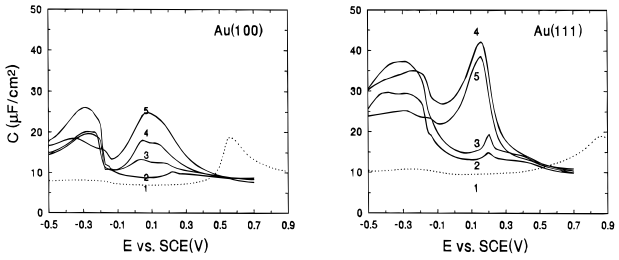

Figure 7. Capacitance vs potentials plots for Au(*hkl*) surfaces in 2.5 mM thymine and 10 mM $KClO_4$ in acetonitrile/water mixtures. Potential steps, 25 mV; acetonitrile content, (1) 100, (2) 0, (3) 5, (4) 13, (5) 19 vol %.

monolayer with the molecular plane oriented parallel to the surface. This latter value has also been found for thymine adsorption on Hg.[34]

We now deal with the deviation from the linear potential vs pH relationship for peak D1, which marks the transition potential from physisorbed to chemisorbed thymine. One possible explanation is based on the higher mobility of protons in solution compared to perchlorate anions. An applied positive (negative) electrode potential leads normally to an accumulation of anions (cations) near the electrode surface. This will be the case in solutions with a medium pH. In solutions with a higher proton concentration (low pH), it is likely that even positive electrode potentials are counterbalanced by elimination of protons rather than by accumulation of anions. This leads to a local increase of the pH in the double layer compared to the bulk solution.

The pH variation has a very different effect on the formation of the physisorbed film which is characterized by peaks F1. In the pH range from 1 to 8, we do not see any changes in the peak position or charge. A further increase of the pH leads to a positive shift of F1, and at a critical pH of 10.10, peaks F1, F2, and F1* totally vanish. This indicates that anions of thymine destabilize the physisorbed film in region II.

3.1.3. Film Formation in Acetonitrile. The reason behind studying film formation in acetonitrile was to determine the role that water plays in the formation of the physisorbed as well as the chemisorbed film. Therefore, we substituted water by acetonitrile, which satisfies the following conditions: (1) the interaction energy with Au is comparable to the one of water, (2) a sufficient solubility of thymine for the film formation (2.5 mM) as well as $KClO_4$ (10 mM), (3) a "water-free" solvent (see Experimental Section). The interaction between acetonitrile and gold has been studied by us both *ex situ* under ultrahigh vacuum conditions[43,44] and *in situ* in an electrochemical cell.[45]

The interaction between acetonitrile and Au(100) can be classified as a physisorption. The desorption temperature of about 172 K, measured by temperature-programmed desorption (TPD), leads to a binding energy of 46 kJ/mol, similar to the one predicted for water on gold (42 kJ/mol[46]). Coadsorption of K on a Au(100) surface slightly increases the adsorption energy of acetonitrile up to 56−73 kJ/mol.[44] The stabilization is mainly due to the formation of coordination shells for acetonitrile centered at K ions. *In situ* infrared reflection measurements also point to weakly adsorbed acetonitrile molecules nearly over the entire potential range.[45] A slight blue shift for the CN valence oscillation at high positive potentials has been observed and can be interpreted as an increase of the acetonitrile−gold interaction.

The above-cited work shows that a substantial replacement of thymine by acetonitrile is highly unlikely to occur. However, the capacitance measurements in Figure 7 of Au(100) and Au(111) in a water/acetonitrile mixture show that the formation of condensed adlayers of thymine is hindered by progressive

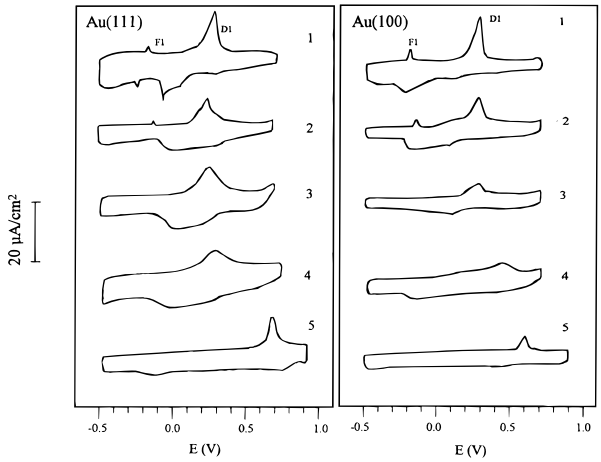

Figure 8. Cyclic voltammograms for Au(*hkl*) surfaces in 2.5 mM thymine and 10 mM $KClO_4$ in acetonitrile/water mixtures. Potential scan, 50 mV/s; acetonitrile content, (1) 0, (2) 19, (3) 40, (4) 91, (5) 100 vol %.

addition of acetonitrile. The well-defined capacitance edge at −0.18 V for both Au(100) and Au(111) crystals in water (Figure 7, curve 2) vanishes if the amount of acetonitrile exceeds 19 vol % (Figure 7, curve 5). At such low acetonitrile concentrations, we only observe a slight influence on the chemisorbed film at more positive potentials. The situation changes drastically if water is completely substituted by acetonitrile (Figure 7, curve 1). The capacitance is significantly lowered nearly over the entire potential range. At very positive potentials, we observe an increase of the capacitance which might be due to the desorption of thymine. The very different capacitance in both solvents indicates that water plays a significant role in the stabilization of both the physisorbed and the chemisorbed films. This is further corroborated by cyclic voltammetry measurements in Figure 8. Peak F1 vanishes at the critical acetonitrile content of 19 vol %. Peak D1 becomes unsymmetrical and broader, its charge is lowered, and the peak position shifts strongly to more positive values with decreasing water content. In pure acetonitrile-containing solutions, we again observe a sharp peak with a significantly lower charge. This peak D1 for Au(100) shows the same characteritics as in thymine-free acetonitrile.[45] It has a charge of $6.5 \pm 0.5\ \mu C/cm^{-2}$ and FWHM of 50 ± 5 mV. This peak has been assigned to the lifting of the reconstruction by perchlorate ions to be the case. The shift of this peak by +0.25 V on thymine addition indicates that thymine is substantially adsorbed. A similar interpretation for D1 at the Au(111) surface fails, since no such peaks have been detected in thymine-free acetonitrile.

3.2. *Ex Situ* Photoelectron Spectroscopy Measurements. XPS measurements have been performed to analyze the chemical state of adsorbed thymine molecules on the (111) surface at different potentials. The main objective was to distinguish the chemisorbed state from the physisorbed adsorption state. It is clear that the emersed adlayer will not represent in every detail the adsorption structure in solution. The bulk of the interfacial water will be removed under vacuum conditions at 293 K. It is of great interest if the adsorbed water which is involved in the hydrogen-bonding network with thymine remains intact upon emersion. In this case, the *ex situ* measurements for the emersed adlayer should give a good representation of the chemical state of the thymine adlayer formed in the electrochemical cell. Nevertheless, the chemical state of thymine molecules in the emersed adlayer should be mainly unperturbed.

As a reference, XPS data of a multilayer thymine were taken. This has been achieved by dipping the electrode in a saturated

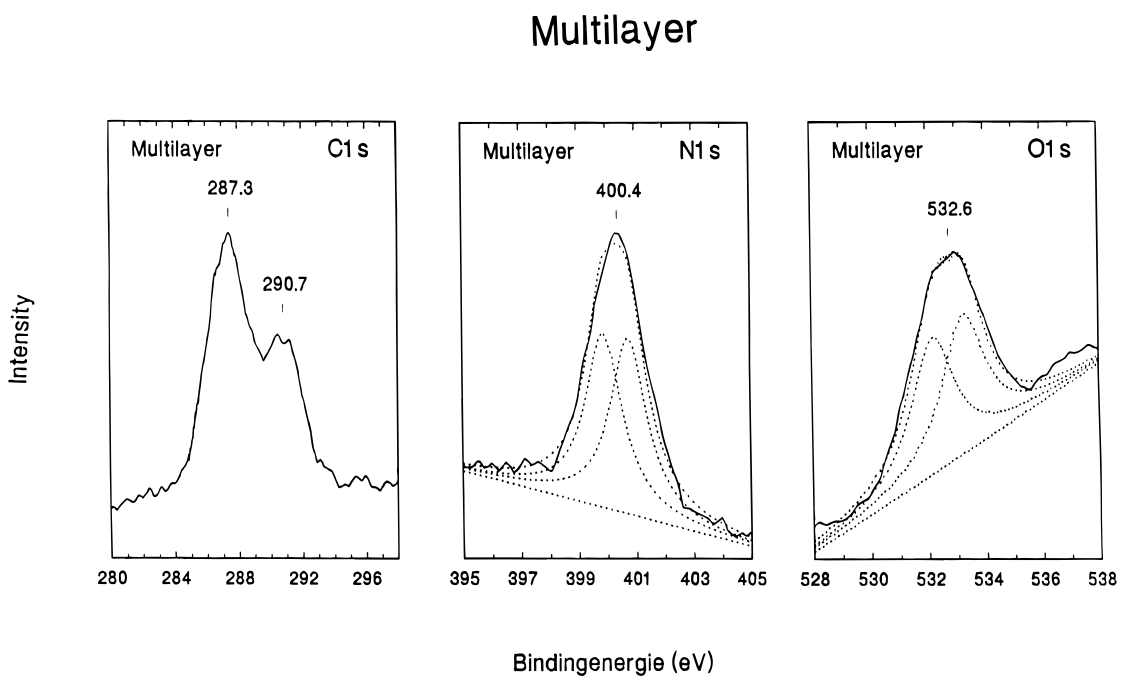

Figure 9. XP spectra of the N 1s, O 1s, and C 1s regions of a multilayer thymine on a Au(111) surface obtained by emersion of the crystal from a saturated thymine solution without potential control.

thymine solution ($c > 30$ mM). After emersion of the probe, a porous white spot of adsorbate on the electrode was visible. Figure 9 shows spectra of this multilayer in the C 1s, N 1s, and O 1s ranges. The C 1s spectrum shows a couple of little resolved peaks arising from the five different carbon atoms. Two major multicomponent peaks at 287.3 ± 0.2 and 290.7 ± 0.2 eV can be clearly distinguished. The latter peak represents the two ketonic carbons.[47] We desist from fitting the signal to five Lorentzian curves since the signal-to-noise ratio is not sufficiently good. Nevertheless, we mentioned here that the observed spectrum is in good agreement to the ones observed by Barber and Clark[47] and Peeling et al.[48]

The N 1s spectrum (full line) shows one single peak at 400.4 ± 0.2 eV. Peeling et al.[48] also observed one single peak from thymine powder at 400.9 ± 0.15 eV, whereas Barber and Clark[47] distinguished two nitrogen signals at 401.1 (N3) and 402.1 ± 0.3 eV (N1), both experimentally and theoretically. The poor peak separation of the two N atoms is due to their very similar chemical states. The single peak in our spectrum can be fitted by two equal Lorentzian curves with a FWHM of 1.52 eV centered at 399.9 and 400.7 ± 0.1 eV (dotted lines). A similar value of 1.5 eV for the FWHM of a N 1s level has been recently reported for a self-assembled monolayer of 6-mercaptopurine on Au(111).[7] The curve centered at lower binding energies can be related to N(3) according to ref 47.

The O 1s spectrum consists of one major peak at 532.6 ± 0.2 eV. This curve can also be fitted by two equal Lorentzian curves with a FWHM of 1.83 eV centered at 532.1 and 533.2 ± 0.1 eV. The powder spectrum of Peeling et al. exhibits one peak at 532.0 ± 0.15 eV.

The intensity ratio between the N 1s, O 1s, and C 1s signals is 2:2:5.4. This is within the expected range with an experimental error of about 10%. However, a slight contamination of the surface with advantitious hydrocarbon cannot be excluded. This is due to the relatively long period between transfer and measurement. Coadsorption of water in the thymine multilayer has not been observed. Therefore, we can exclude the formation of thymine monohydrate, which has been prepared from aqueous solutions and characterized by X-ray diffraction.[49] The potential-dependent XPS measurements have been performed with a 1 mM thymine solution in 10 mM perchloric acid. This concentration has been chosen to avoid multilayers on the emersed electrode. Multilayers may arise from emersion with an additional adhering liquid layer if the solution concentration is too high. Lower concentrations reduce the signal-to-noise ratio over a wide potential range.

Figure 10 shows the XP spectra after emersion of the Au(111) electrode at three different potentials which reflect three different adsorption states according to cyclic voltammetry and capacitance−potential measurements. The spectrum recorded at 0.52 V represents the chemisorbed film, the spectrum at 0.17 V the condensed physisorbed film, and the spectrum at −0.38 V the noncondensed physisorbed adsorption state. The most significant changes with the potential are visible in the N 1s spectra. A significant splitting of the two N 1s signals (1.5 ± 0.2 eV) is observed for the chemisorbed adlayer, whereas the physisorbed adsorption states at negative potentials show a comparable peak splitting (0.7 ± 0.1 eV) to the multilayer spectra.

All N 1s spectra are fitted with two equal Lorentzian curves with the same FWHM (1.52 eV) as for the multilayer spectra. The shift of one N 1s signal compared to the other N 1s signal to lower binding energies is due to an increase in electron density at this nitrogen atom. This may be achieved either by deprotonation or by keto−enol tautomerism. For the keto−enol tautomerism, a shift of about 1.5 eV to lower binding energies is expected.[48] Comparing the spectra with the multilayer spectrum leads to observation that there are shifts to lower binding energies for all emersion potentials. This shift is about 0.4−1.0 eV depending slightly on the emersion potential. The shift might be due to an extra-atomic relaxation shift (ΔE_r) of the photoelectrons in the multilayer (see, e.g., ref 50). We will return to this point later on. For the O 1s signal, we desist from further fitting due to the poor signal-to-noise ratio and an extra contribution to the signal from coadsorbed perchlorate ions. As for the N 1s spectra, a general shift to lower binding energies compared with the multilayer spectrum is observed. The position of the main peak containing two oxygen signals is 530.7 ± 0.3 eV, shifted by about 1.9 ± 0.3 eV to lower binding energies (see Table 1), independent of the potential. This shift

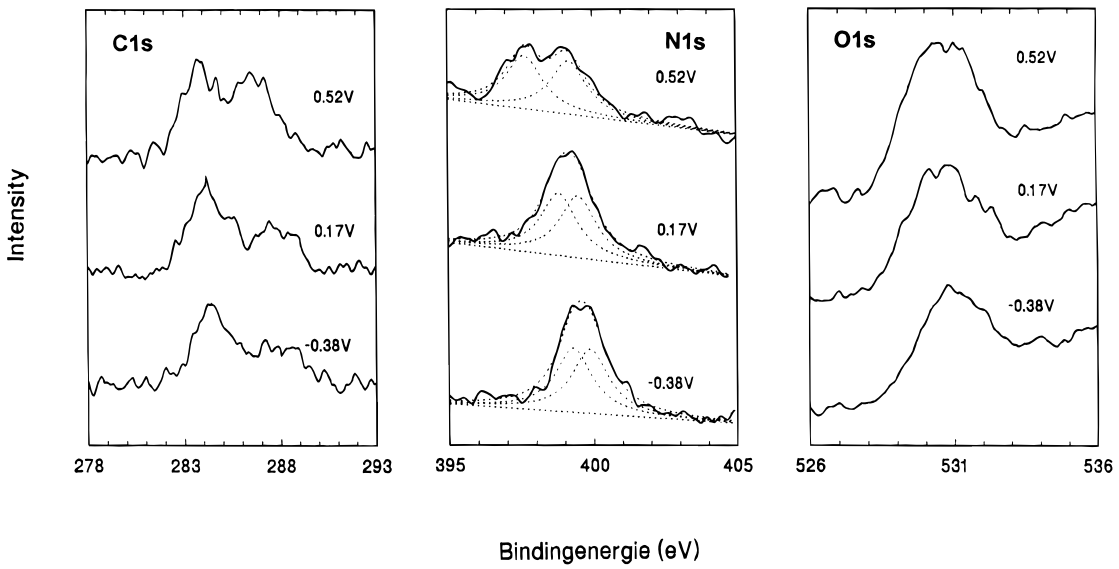

Figure 10. XP spectra of the N 1s, O 1s, and C 1s regions after emersion of the Au(111) electrode from a 1 mM thymine/10 mM $HClO_4$ containing solution at three different potentials.

TABLE 1: Measured Peak Positions and Shifts ΔE between the Multi- and Monolayers of the N 1s, O 1s, and C 1s Core Level Spectra (No Fitted Values)[a]

core level	multilayer ± 0.1 eV	monolayer ± 0.3 eV	$\Delta E \pm 0.4$ eV
N 1s	400.4	399.4−399.8	0.6−1.0
O 1s	532.6	530.7	1.9
C 1s 1st peak	287.3	284.2	3.1
2nd peak	290.7	287.7	3.0

[a] For the N 1s levels, only spectra which show a single peak are considered (for Emersion potentials, $E < 0.4$ V).

seems too large to be attributed to extra-atomic relaxation in the multilayer which has been found in the range from 0.1 to 0.7 eV.[50]

The two major peaks in the C 1s spectra show a strong dependence on the emersion potential. The peak splitting at potentials $E < 0.20$ V is about 3.5 ± 0.3 eV, comparable to the multilayer spectra ($\Delta E = 3.4$ eV). For the emersion potentials, $E > 0.2$ V, which reflect the chemisorbed film, we observe a substantial decrease of the peak splitting down to 2.5 ± 0.3 eV, mainly due to a shift of the second peak to lower binding energies. The shift of the second peak by about 1 eV to lower binding energies suggests the existence of enolic carbon rather than the ketonic carbon. Experimental and theoretical studies of some model compounds have revealed a shift of 1 eV to lower binding energies for the enolic form.[51] Apart from this, we observe for all emersion potentials a shift of about $\Delta E = 3.1$ eV to lower binding energies. Some limitations in the interpretation of the C 1s data stem from adsorption of additional hydrocarbons. Since the hydrocarbon contamination contributes to a constant increase of the signal strength at 284.6 eV, the peak separation between the two major peaks should be independent of this contamination.

For physisorbed molecules in a multilayer, one would expect a constant extra-atomic relaxation shift (ΔE_r) of about 0.1−0.7 eV in the multilayer for all core levels of C, N, and O, as has been shown for different molecules by Sexton and Hughes.[50] The surprisingly large ΔE shift for the C 1s and O 1s levels suggests a mechanism other than extra-atomic relaxation. Comparable shifts of monolayers to lower binding energies have been obtained for dimethyl disulfide on Au(111)[52] and acetonitrile on Pt(111).[50] These shifts have been interpreted by chemisorption of the adsorbate in which rehybridization of the

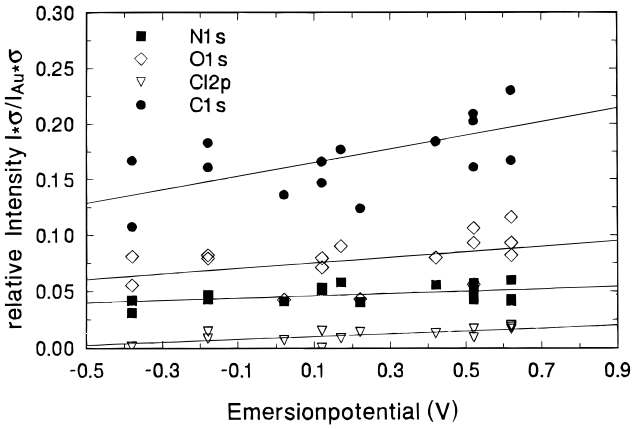

Figure 11. Intensities of the N 1s, O 1s, C 1s and Cl 2p signals divided by the atomic sensitivity factors and relative to the Au($4f_{7/2}$) signal.

adsorbate bondings occurs. We have to assume, therefore, that thymine is chemisorbed on the Au(111) after emersion either at negative and at positive electrode potentials under the special ultrahigh vacuum conditions. These findings are in contrast to the interpretation of the electrochemical investigations which point to a weakly adsorbed thymine adlayer at potentials negative of the Epzc. This difference might be induced by the evaporation of the solvent. Therefore, measurements at low temperatures with coadsorbed water would be very helpful.

Additional spectra of the Cl 2p level have been recorded to analyze coadsorption of anions on the one hand and to explain additional oxygen in the O 1s spectra on the other hand. Analyses are made somewhat difficult due to the very low amount of perchlorate.

The relative intensities of the N 1s, O 1s, C 1s, and Cl 2p level are presented in Figure 11. The low intensity ratios for all species suggest adsorption of thymine in the submonolayer range. This might be due to an incomplete dissolution of the film during the emersion process, which would also explain the relatively large scattering of the signal strength.

There are only slight changes observed upon changing the potential. At negative and medium potentials *($E < 0.2$ V)*, we detect constant N 1s, C 1s, and O 1s levels. An increase of about 20% in the intensity is observed for the O 1s and C 1s signal for the most positive potentials ($E \geq 0.2$ *V*). For the N 1s signal, a comparable increase cannot be observed due to the

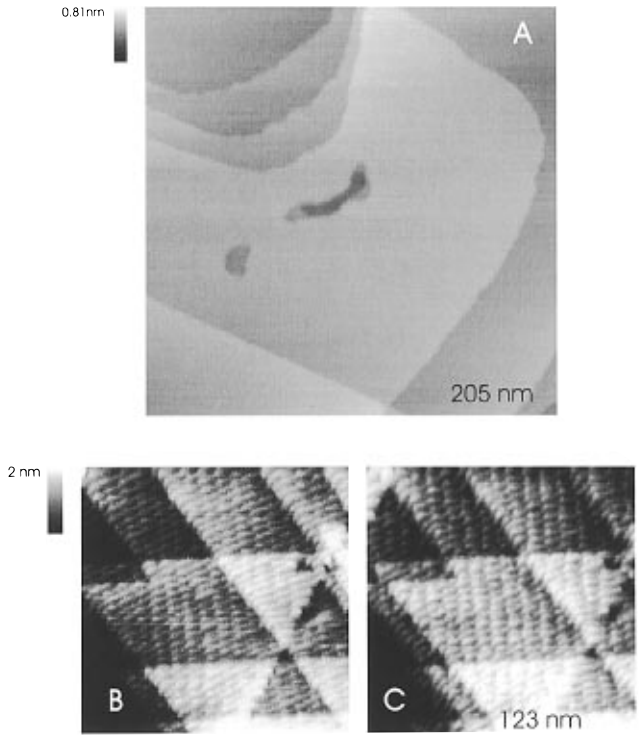

Figure 12. Large scan *in situ* STM images of the Au(111) surface in (a) pure $HClO_4$ electrolyte at −0.05 V, (b) with 5 mM thymine at −0.05 V, and (c) with 5 mM thymine at +0.5 V. All images were taken in constant current mode. $V_{Bias} = -0.04$ V, $I_t = 5.2$ nA, 123 nm × 123 nm for b and c, $V_{Bias} = -0.01$ V, $I_t = 4.8$ nA for 205 nm × 205 nm for a.

high scattering of the signal. The relative N 1s intensity is scattered around 0.045−0.055. This is about the same as for a Au(111) electrode emersed from pyrazine-containing solutions.[53] The N 1s to O 1s ratio is 1, taking into account the additional intensity of adsorbed perchlorate ions. Again we have to assume that water molecules are not present at the emersed electrode. The N 1s to C 1s ratio is about 1 to 3.5 instead of 1 to 2.5 for the pure thymine adlayer, indicating contamination by hydrocarbons, which may be due to the relatively long period between emersion and measurement. The effect of hydrocarbon adsorption leads to a constant contribution at 284.6 eV[54] for all emersion potentials and should therefore only influence marginally the interpretation of our measurements. The most striking feature in Figure 11 is the low and nearly constant amount of adsorbed perchlorate ions. Between −0.2 and +0.4 V, only a very slight increase of anions can be detected. This may arise if the potential drop in the adlayer is mainly governed by the proton concentration rather than by ClO_4^-. This corroborates the electrochemical interpretation concerning the electron transfer in peak D1.

Additional measurements in $KClO_4$-containing solutions instead of perchloric acid show very similar results concerning the peak splitting for the N 1s spectra. However, these measurements do not show the desired precision, which may be due to the emersion of an additional adhering liquid layer.

3.3. *In Situ* Scanning Tunneling Microscopy of Adsorbed Thymine. *In Situ* STM images of a Au(111) surface in thymine-free and thymine-containing solutions for large scan ranges are shown in Figure 12. The images have similar *z* scaling. Figure 12a shows the Au(111) surface in 0.01 M perchloric acid. Large terraces with monoatomic steps with a height of 0.24 nm are clearly resolved. The terraces are smooth and atomically flat. At negative potentials, there is a very slight *z* corrogation of about ±0.02 nm arising from the formation of reconstruction rows.[55] These reconstruction rows have a zigzag pattern and are separated by 6.7 nm. The STM pattern dramatically changes upon thymine addition, either at potentials where the physisorbed film is formed (Figure 12b) or at more positive potentials where the chemisorbed film (Figure 12c) is formed. We assign this change to the adsorption of thymine on the electrode in both potential regions. This is in contrast to the measurements of Tao et al.,[9] who only observed adsorption of thymine at positive potentials. We do not see any differences in the STM images for the chemisorbed film and the physisorbed film in the large scan ranges. Differences can only be observed in high-resolution or molecular resolution STM images, which are presented and discussed in the following section. In every case, a complete adsorption of thymine over the entire electrode area was observed. Thymine-free and thymine-covered electrode areas were never simultaneously observed. The thymine-covered electrode nevertheless shows some characteristics of the uncovered surface. The angles between the terrace edges are $n \times 60°$, typical for the (111) surface, and the steps show a height of 0.24 nm. These observations point to an adsorption somewhere between a submonolayer of thymine to a few monolayers at most.

3.3.1. High-Resolution STM Images of the Physisorbed Film. Figure 13a shows an unfiltered STM imge of the Au(111) electrode in thymine-containing solutions at 0.12 V. This image shows a highly periodic pattern, different from the underlying gold lattice. From the STM image, we can construct a unit cell, illustrated by solid black lines. The measured lattice constants are $a = 0.95 \pm 0.03$ nm, $b = 1.01 \pm 0.03$ nm, and $\gamma = 57 \pm 3°$. The lattice constants do not fit the lattice constants of the underlying gold substrate of 2.89×2.89 nm^2. These images are consistent with thymine forming an incommensurate overstructure. This has already been concluded from the electrochemical measurements.

In the STM pattern, ringlike patterns occur which have the same dimensions as a flat-lying thymine molecule. This is demonstrated in Figure 13b in which ball-and-stick models of thymine are superimposed upon the STM image. The thymine models fit perfectly to the ringlike structures. These ringlike structures indeed appear to reflect the likely electronic density of a flat-oriented thymine molecule. The lowest electronic density in the HOMO of thymine occurs at the N(1) atom. We placed this atom at the position where the lowest tunneling current in the ring structure occurs. An occupation of all the ringlike structures in the STM images by thymine molecules leads to a surface excess of only 1.7×10^{-10} mol cm^{-2}, which seems definitely too low for a condensed adlayer. Moreover, an intermolecular stabilization effect by a hydrogen-bonding network including thymine alone is very difficult to imagine. The additional spots in the STM images cannot be attributed to gold atoms since the spacings between the spots do not fit with the underlying substrate lattice. It is also possible that additional water molecules may stabilize this adsorption structure, or on the other hand, it is possible that the film consist not only of one monolayer but also of a second or third adsorption layer. The former assumption is strongly corroborated by the electrochemical measurements. The latter assumption nevertheless might fit better to the observed STM image since additional thymine molecules can be constructed under the first layer. From our measurements, we cannot exclude one of these possibilities. We have to leave this point open for further measurements with similar molecules like uracil and its derivatives.

3.3.2. High-Resolution STM Images of the Chemisorbed Film. Figure 14a and b shows an unfiltered and a Fourier-transformation-filtered STM image of the chemisorbed film at

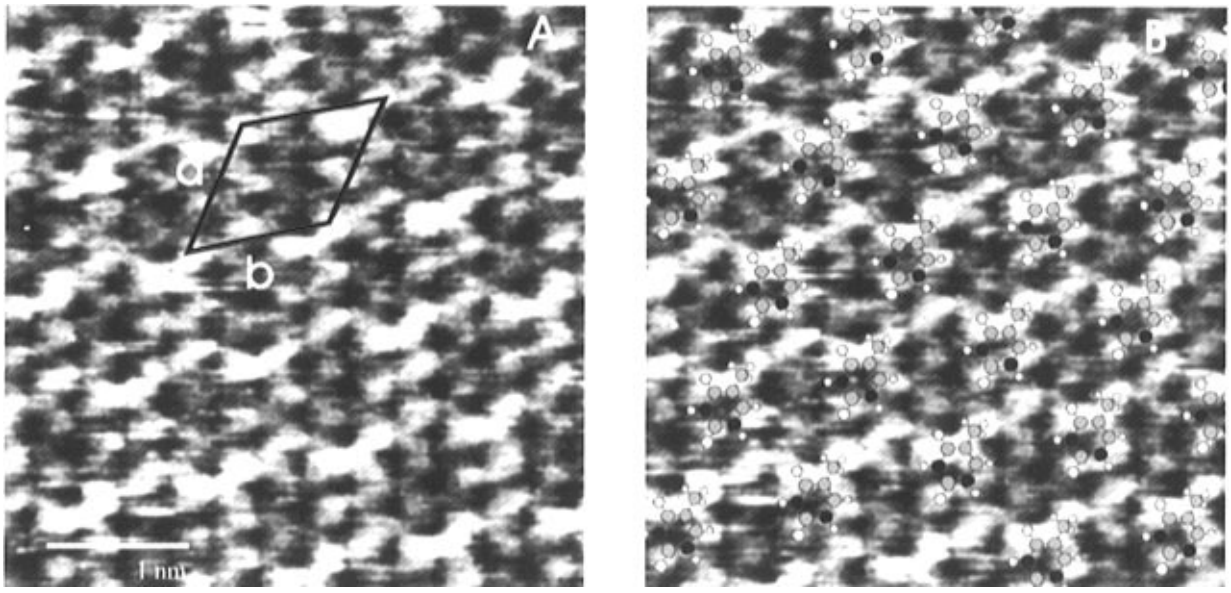

Figure 13. (a) Unfiltered high-resolution STM images of a Au(111) surface in 5 mM thymine and 10 mM $HClO_4$ at 0.12 V. $V_{Bias} = -0.04$ V, $I_t = 12.1$ nA, constant current mode. (b) Same as a and covered with ball-and-stick models of thymine.

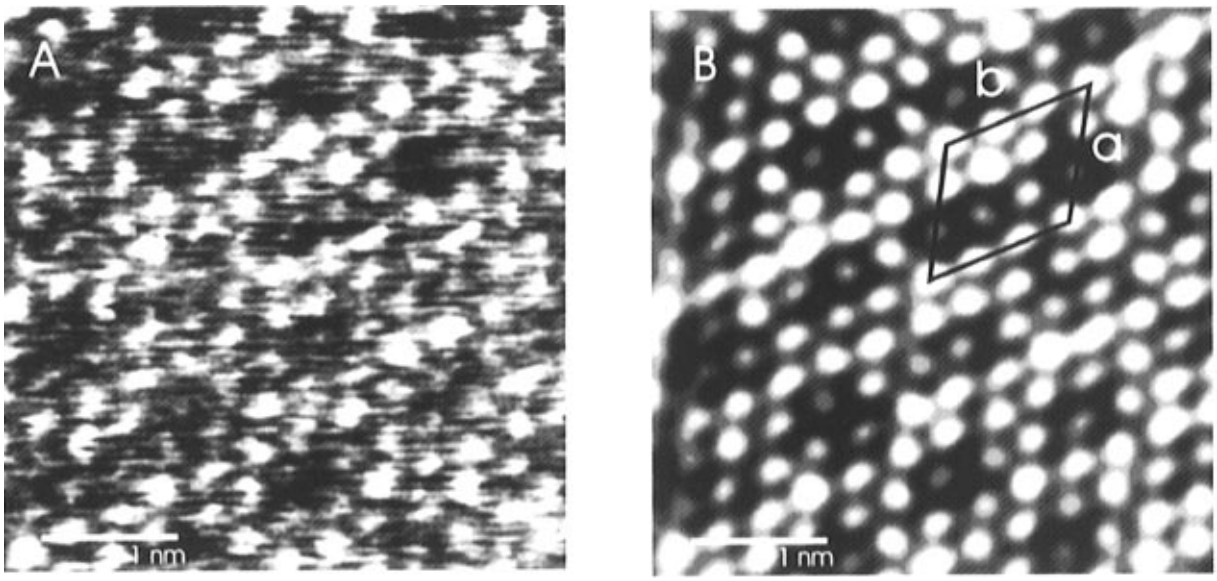

Figure 14. Unfiltered (a) and filtered (b) high-resolution STM images of a Au(111) surface in 5 mM thymine and 10 mM $HClO_4$ at 0.5 V. $V_{Bias} = -0.04$ V, $I_t = 10.9$ nA, constant current mode.

0.5 V. This STM image also shows a highly periodic structure with a unit cell of the following dimensions: $a = 0.99 \pm 0.03$ nm, $b = 1.02 \pm 0.03$ nm, and $\gamma = 62 \pm 3°$. This unit cell has a slightly larger unit cell than the physisorbed film. The cell dimensions might be expressed by $2\sqrt{3} \times 2\sqrt{3}\ R30°$ in units of the underlying substrate lattice. The spacings between all spots in direction a are 0.33 ± 0.02 nm and in direction $b = 0.34 \pm 0.02$ nm. The pattern consists of rows of bright double spots which are separated by a line of single medium-bright spots. From this image, we constructed a model of the chemisorbed film, the two variations of which are presented in Figure 15a and b. This model takes not only the STM but also the XPS and electrochemical measurements into account. Thymine and water molecules are represented by space fill models, and the substrate is depicted by a hard-sphere model. In this model, thymine and water molecules form a densely packed overlayer. Thymine molecules are oriented with their molecular plane perpendicular to the surface. The deprotonated N(3) atom of each molecule points to the surface. Thymine molecules are bridged by water molecules along the a axis, whereas an infinite chain of molecules is formed along the b axis. This latter chain is built by stacks of molecules in which the intermolecular spacing is 0.34 nm. This spacing corresponds very well with the distance between the spots in the STM image and the crystallographic data of thymine monohydrate.[49] Thymine molecules in the monohydrate also arrange into stacks in which the distance between these molecules is 0.34 nm.

The assumption that water molecules are incorporated in the chemisorbed film is further corroborated by a similar observation of Allen and co-workers,[6] who found a similar adsorption geometry for the self-assembled adenine adlayer on HOPG. Thymine molecules could possibly adopt either the enolic or the ketonic form. Our model can be applied to both mesomeric forms, as it is shown in Figure 15a and b. For the enolic form, it is necessary that the water molecules be oriented with the O atom pointing directly to the surface, with its molecular plane perpendicular to the one of thymine. In the ketonic form, the oxygen end of water molecules points away from the surface and each molecule is in line with thymine molecules. Figure 15c illustrates the latter case. A cross section through the model

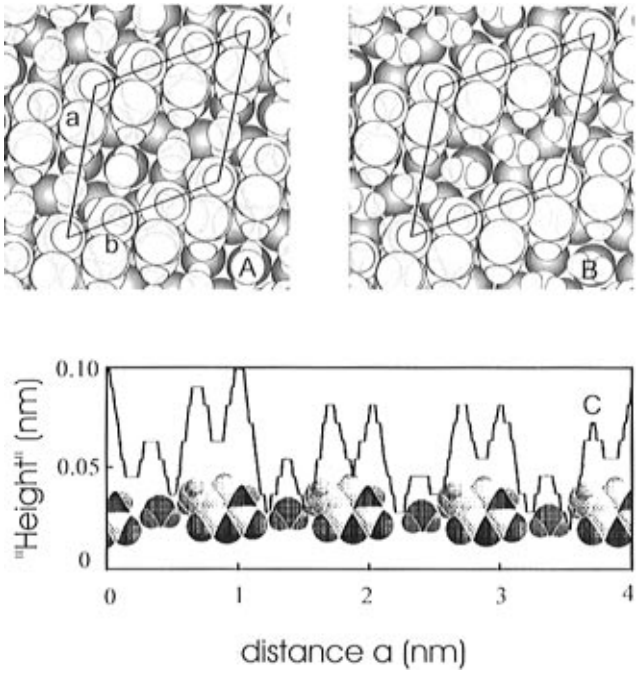

Figure 15. Models for thymine adsorption at the interface at 0.5 V. The balls represent the Au(111) surface; thymine and water molecules are represented by space fill models (a) Model for the dioxotautomeric form and (b) for the enolic form. (c) Cross section through the STM image and the model along the *a* axis (see Figure 14).

is compared with the analogous cross section through the STM image along the *a* axis. The two main tunneling maxima can be assigned to the thymine molecule, whereas the little maxima in between coincide with the position of water molecules.

The orientation of the thymine rows with respect to the substrate lattice is difficult to determine, because of the abovementioned difficulties in observing thymine and substrate simultaneously. This aspect of our model is mainly developed on the basis that the lattice vectors can be expressed by $2\sqrt{3} \times 2\sqrt{3}$ in terms of the substrate lattice. This includes a rotation of 30° for the adsorbate unit cell with respect to the substrate. Additional evidence stems from the model itself. The intensity of the spots corresponding to water varies in the STM unit cell, but the intensity variation shows periodicity with every fourth spot having similar intensity. In a $2\sqrt{3} \times 2\sqrt{3}\ R30°$ unit cell, every fourth water molecule occupies the same adsorption site above the gold lattice. The water molecules in between are placed above different adsorption sites. This may influence the tunneling characteristics of the water molecule and give rise to the periodic variation in the spot intensity.

Our model leads to a surface excess of 5.0×10^{-10} mol/cm^2, which is in full agreement with the electrochemical data.

The question arises why it is possible to assign some of the STM spots for the chemisorbed film to water molecules, whereas no such assignment can be done for the STM pattern of the physisorbed film? A possible explanation can be drawn from the different behavior of the films in water/acetonitrile mixtures. The physisorbed film dissolutes at low acetonitrile concentrations, whereas the chemisorbed film is destroyed only if water is completely substituted. The formation of a nearly complete water inner layer at the electrode and, therefore, a complex water network around the adsorbate molecules could be necessary for the formation of the physisorbed but not for the chemisorbed film.

From this point of view, it is likely that for the chemisorbed film, water molecules are directly incorporated in the film. The interpretation of our STM images is consistent with the assumption that incorporated water molecules are highly immobilized. Water molecules in our model (Figure 15) are fixed by two thymine molecules, and this could be the reason for the possibility to image water molecules.

For the formation of the physisorbed film, a nearly complete water network at the electrode surface may be necessary. This includes that the stabilization effect of water on the film is not necessarily based on immobilized or really incorporated water molecules, which give rive to additional spots in the STM image. The stabilization effect is likely due to the hydration of both the electrode and the thymine molecules.

Switching the potentials between the two adsorption regions II (physisorbed film) and III (chemisorbed film) leads to a slow transformation of the STM images into each other. It was not possible to observe the transformation process in one STM image. This transformation process took several minutes.

4. Summary

We have examined the adsorption of thymine on three different Au electrodes with classical electrochemical methods. *Ex situ* XPS and *in situ* STM measurements have been performed to analyze the adsorption of thymine on Au(111). The electrochemical data reveal three different adsorption states which depend strongly on solution concentration, temperature, electrode potential, the nature of the solvent, and the solution pH. The three adsorption states can be classified as (I) a random, (II) a condensed, and (III) a condensed, chemically modified adlayer. Adsorption states I and III occur on all electrodes, whereas state II only exists on the reconstructed Au(100) and (111) surface. Transformation from state II into the condensed, chemically modified adlayer takes place *via charge transfer* from deprotonated thymine molecules to the gold surface. This interpretation is confirmed by the XPS measurements on the (111) electrode, which show a significant shift of one N(3) core level for thymine in adsorption state III. High-resolution *in situ* STM measurements on the same electrode show two different ordered adsorption layers of thymine for adsorption states II and III. State II involves flat-lying molecules in a unit cell with $a = 0.95 \pm 0.03$ nm, $b = 1.01 \pm 0.03$ nm, and $\gamma = 57 \pm 3°$. A simple monolayer adsorption model fails to explain all features of the STM pattern. For adsorption state III with unit cell dimensions $a = 0.99 \pm 0.3$ nm, $b = 1.02 \pm 0.3$ nm, and $\gamma = 62 \pm 3°$, an adsorption model has been developed which accounts for all the electrochemical, XPS, and STM data. This model contains upright standing thymine molecules connected via N(3) atoms to the surface. The thymine molecules form rows which are connected by hydrogen-bonding water molecules. The surface excess for this model comes to $5.0 \pm 0.5 \times 10^{-10}$ mol cm^{-2}, which is in good agreement with the electrochemical data.

Acknowledgment. Financial support of this work by the Deutsche Forschungsgemeinschaft is gratefully acknowledged.

References and Notes

(1) Lorenz, W. *Z. Elektrochem.* **1958**, *62*.
(2) Armstrong, R. D. *J. Electroanal. Chem.* **1969**, *20*, 168.
(3) Sathyaranayana, S. *J. Electroanal. Chem.* **1965**, *10*, 56.
(4) Vetterl, V. *Collect. Czech. Chem. Commun.* **1966**, *31*, 2105.
(5) Bain, C. D.; Whitesides, G. M. *Angew. Chem., Int. Ed. Engl.* **1989**, *28*, 506.
(6) Allen, M. J.; Balooch, M.; Subbiah, S.; Tench, R. J.; Siekhaus, W.; Balhorn, R. *Scanning Microscopy* **1991**, *5*, 625.
(7) Boland, T.; Ratner, B. D. *Langmuir* **1994**, *10*, 3845.
(8) Batrakov, V. V.; Damaskin, B. B.; Ipatov, U. P. *Elektrokhim.* **1974**, *10*, 144.
(9) Tao, N. J.; DeRose, J. A.; Lindsay, S. M. *J. Phys. Chem.* **1993**, *97*, 910.

(10) Wandlowski, Th. *J. Electroanal. Chem.* **1995**, *395*, 83.
(11) Hölzle, M. H.; Wandlowski, Th.; Kolb, D. M. *Surf. Sci.* **1995**, *335*, 281.
(12) Hamelin, A.; Morin, S.; Richer, J.; Lipkowski, J. *J. Electroanal. Chem.* **1991**, *304*, 195.
(13) Scharfe, M.; Hamelin, A.; Buess-Herman, C. *Electrochim. Acta* **1995**, *40*, 61.
(14) Buess-Herman, C. In *Adsorption of Molecules at Metal Electrodes*; Lipkowski, J., Ross, P. N., Eds., VCH: New York, 1992; Chapter 2.
(15) Buess-Herman, C. *Prog. Surf. Sci.* **1994**, *46*, 335.
(16) Lipkowski, J.; Stolberg, L. In *Adsorption of Molecules at Metal Electrodes*; Lipkowski, J., Ross, P. N., Eds.; VCH: New York, 1992; Chapter 2.
(17) Fleischmann, M.; Hendra, P. J.; McQuillan, A. J. *J. Chem. Soc., Commun.* **1973**, *3*, 80.
(18) Fleischmann, M.; Hendra, P. J.; McQuillan, A. J. *Chem. Phys. Lett.* **1974**, *26*, 163.
(19) Mark, H. B.; Pons, S. B. *Anal. Chem.* **1966**, *38*, 119.
(20) Ashley, K.; Pons, S. *Chem. Rev.* **1988**, *88*, 673.
(21) Nichols, R. J. In *Adsorption of Molecules at Metal Electrodes*; Lipkowski, J., Ross, P. N., Eds.; VCH: New York, 1992; Chapter 7.
(22) Binnig, G.; Rohrer, H.; Gerber, C.; Weibel, E. *Appl. Phys. Lett.* **1982**, *40*, 178.
(23) Chang, S. Molecular imaging by STM. In *Scanning Tunneling Microscopy I*; Springer Series in Surface Sciences 20; Güntherodt, H.-J., Wiesendanger, R., Eds.; Springer Verlag: New York, 1991.
(24) Sass, J. K.; Kretschmar, K. *Vacuum*, **1981**, *31*, 483.
(25) Wagner, F. T. In *Structure of Electrified Interfaces*; Lipkowski, J., Ross, P. N., Eds.; VCH: New York, 1993; Chapter 9.
(26) Bunge, E.; Nichols, R. J.; Baumgärtel, H.; Meyer, H. *Ber. Bunsenges. Phys. Chem.* **1995**, *99*, 1243.
(27) Bunge, E.; Nichols, R. J.; Roelfs, B.; Meyer, H.; Baumgärtel, H. *Langmuir* **1996**, *12*, 3060.
(28) Roelfs, B.; Baumgärtel, H. *Ber. Bunsenges. Phys. Chem.* **1995**, *99*, 677.
(29) Haiss, W.; Lackey, D.; Sass, J. K.; Besocke, K. H. *J. Chem. Phys.* **1991**, *95*, 2193.
(30) Haiss, W.; Lackey, D.; Sass, J. K.; Meyer, H.; Nichols, R. J. *Chem. Phys. Lett.* **1992**, *343*, 200, No. 4.
(31) Damaskin, B. B.; Petrii, O. A.; Batrakov, V. V. *Adsorption of Organic Compounds on Electrodes*; Plenum: New York, 1971.
(32) Sridharan, R.; de Levie, R. *J. Electroanal. Chem.* **1986**, *201*, 133.
(33) Sridharan, R.; de Levie, R. *J. Phys. Chem.* **1986**, *86*, 4489.
(34) Saffarian, M. H.; Sridharan R.; de Levie, R. *J. Electroanal. Chem.* **1987**, *218*, 273.
(35) Kolb, D. M. In *Structure of Electrified Interfaces*; Lipkowski, J.; Ross, P. N. Eds.; VCH: New York, 1993; Chapter 3, Bd. 2, p 65.
(36) Hölzle, M. H.; Wandlowski, Th.; Kolb, D. M. *J. Electroanal. Chem.* **1995**, *394*, 271.
(37) Rikvold, P. A.; Gamboa-Aldeco, M.; Zhang, J.; Han, M.; Wang, Q.; Richards, H. L.; Wieckowski, A. *Surf. Sci.* **1995**, *335*, 389.
(38) Manousek, O.; Zuman, P. *Collect. Czech. Chem. Commun.* **1955**, *20*, 1340.
(39) Shugar, D.; Fox, J. J. *Biochim. Biophys. Acta* **1952**, *9*, 199.
(40) Levene, P. A.; Bass, L. W.; Simms, H. S. *J. Biol. Chem.* **1926**, *70*, 229.
(41) Jovanovic, S. V.; Simic, M. G. *J. Phys. Chem.* **1986**, *90*, 975.
(42) Angerstein-Kozlowska, H.; Conway, B. E.; Hamelin, A.; Stoicoviciu, L. *Electrochim. Acta* **1986**, *31*, 1051.
(43) Solomun, T.; Christmann, K.; Baumgärtel, H. *J. Phys. Chem.* **1989**, *93*, 7199.
(44) Solomun, T.; Baumgärtel, H.; Christmann, K. *J. Phys. Chem.* **1991**, *95*, 10041.
(45) Panzram, E.; Baumgärtel, H.; Roelfs, B.; Schröter, C.; Solomun, T. *Ber. Bunsenges. Phys. Chem.* **1995**, *99*, 827.
(46) Thiel, P. A.; Madey, T. E. *Surf. Sci. Rep.* **1987**, *7*, 211.
(47) Barber, M.; Clark, D. T. *Chem. Commun.* **1970**, 24.
(48) Peeling, J.; Hruska, F. E.; McIntyre, N. S. *Can. J. Chem.* **1978**, *56*, 1555.
(49) Gerdil, R. *Acta Crystallogr.* **1961**, *14*, 333.
(50) Sexton, B. A.; Hughes, A. E. *Surf. Sci.* **1984**, *227*, 140.
(51) Clark, D. T. In *Electron Emission Spectroscopy*; Dekeyser, W., Ed.; Reidel, D.: Dordrecht, Netherlands, 1973; p 373.
(52) Nuzzo, R. G.; Zegarski, B. R.; Dubois, L. H. *J. Am. Chem. Soc.* **1987**, *109*, 733.
(53) Lazarescu, V. *Surf. Sci.* **1995**, *335*, 221.
(54) Wagner, C. D.; Riggs, W. M.; Davies, L. E.; Moulder, J. F.; Muilenberg, G. E. *Handbook of X-Ray Photoelectron Spectroscopy*; Perkin-Elmer: Eden Prairie, MN, 1978.
(55) Gao, X.; Hamelin, A.; Weaver, M. J. *J. Chem. Phys.* **1991**, *95*, 6993.